Isomer ratio measurements as a probe of the dynamics of breakup and incomplete fusion

L. R. Gasques, M. Dasgupta, D. J. Hinde, T. Peatey,[*] A. Diaz-Torres, and J. O. Newton

Department of Nuclear Physics, Research School of Physical Sciences and Engineering,

Australian National University, Canberra, ACT 0200, Australia

(Received 10 October 2006; published 22 December 2006)

The incomplete fusion mechanism following breakup of ^{6,7}Li and ^{9}Be projectiles incident on targets of ^{209}Bi and ^{208}Pb is investigated through isomer ratio measurements for the ^{212}At and ^{211}Po products. The phenomenological analysis presented in this paper indicates that incomplete fusion brings relatively more angular momentum into the system than equivalent reactions with a direct beam of the fused fragment. This is attributed to the trajectories of breakup fragments. Calculations with a 3D classical trajectory model support this. Isomer ratio measurements for incomplete fusion reactions can provide a test of new theoretical models of breakup and fusion.

I. INTRODUCTION

The influence of breakup on fusion and other reaction processes is currently a hot topic for both theoretical and experimental investigation. In the simplest framework, fusion between two nuclei occurs when the projectile overcomes the barrier resulting from the sum of the long-range repulsive Coulomb potential and the short-range attractive nuclear potential. However, the situation gets more complicated in dealing with weakly bound nuclei, since they may break up before reaching the target nucleus. In this situation, two different fusion processes are possible: (i) complete fusion (CF), defined in principle as the capture of all the mass of the projectile by the target, and (ii) incomplete fusion (ICF), which occurs when not all the fragments are captured by the target. Although the reaction mechanism for well-bound stable beams leading to CF is now rather well understood [1], currently no theoretical model can fully describe CF and ICF in reactions involving weakly bound nuclei [2]. The interaction between the two (or more) breakup fragments and the target makes this three (or more) body problem very complex.

Despite the absence of a full theoretical model, breakup can be investigated experimentally, and the results can help in elucidating the important parameters that must be included in a model, for instance whether the trajectories of the fragments after breakup affect measurable quantities. Light stable nuclei such as ^{6,7}Li and ^{9}Be are suitable to investigate the fusion and breakup mechanisms, since accelerated beams can be produced with high intensities, they have low breakup thresholds, and they break up into charged fragments. Reliable interpretation of experimental measurements require CF and ICF products to be identified unambiguously. Since CF and ICF mechanisms lead to different compound nuclei, clear experimental identification is possible, provided the evaporation process following CF does not also populate the ICF evaporation products. The products can be detected by measuring, for example, characteristic γ rays [3–7] or x rays [8–12] or by their ground-state α decay [13–16].

In this paper we investigate the ICF mechanism following breakup of ^{6,7}Li and ^{9}Be projectiles incident on targets of ^{209}Bi and ^{208}Pb by studying the angular momentum distribution of the ICF products. These systems were chosen because the ICF products ^{212}At and ^{211}Po have high-spin isomers that decay by α-particle emission. Both isomeric- and ground-state cross sections could be measured, allowing the determination of isomer ratios [17], which we define as the population of the isomeric state divided by the population of the ground state. The isomer ratios are sensitive to the angular momentum distributions brought into the system. Furthermore, extensive CF and ICF cross-section measurements are available [14–16]. Crucially, isomer ratio data are available for the $\alpha + {}^{208}$Pb and $\alpha + {}^{209}$Bi [18,19] reactions. These lead to the same compound nuclei as are formed by ICF of ^{6,7}Li and ^{9}Be projectiles. Thus the angular momentum brought in for the ICF process can be compared to those in the direct α-beam reactions, which are well understood. The latter are referred to as the calibration reactions.

We first carry out a phenomenological analysis of the measured isomer ratios for the calibration reactions. This analysis is then extended to predict the isomer ratios for the ICF reactions to investigate the effect of the breakup on the angular momentum distribution.

II. EXPECTED PRODUCTS AND CALIBRATION REACTIONS

Complete fusion of ^{6}Li, ^{7}Li incident on ^{209}Bi, and ^{9}Be incident on ^{208}Pb produce the compound nuclei ^{215}Rn, ^{216}Rn, and ^{217}Rn, respectively. Neutron evaporation is the overwhelming decay mode [16], producing residual Rn nuclei that are α-active. For the ICF reactions, the At and Po evaporation residues formed after neutron emission are α-active as well. The different α-decay energies of the residues allow for unique identification. Thus, CF and ICF products can be separately identified and their cross sections can be determined by analysis of the α-decay spectra. The only exception is the ICF product resulting from absorption of ^{8}Be from the possible breakup of ^{9}Be, which cannot be separated from CF of ^{9}Be.

---

[*]Present address: Bureau of Meteorology, Regional Office Queensland, Brisbane, QLD 4001, Australia.

In this work we are interested specifically in ^{212}At and ^{211}Po, having isomeric states at 0.223 MeV with spin 9^- and at 1.462 MeV with spin $(25/2)^+$, respectively. Their formation and the corresponding calibration reactions are as follows:

(i) The nucleus ^{6}Li may break up into an α particle and a deuteron (with a separation energy $S_\alpha = 1.48$ MeV). Capture of the α particle by ^{209}Bi results in ^{213}At, which after $1n$ evaporation forms ^{212}At. The corresponding calibration reaction is $\alpha + ^{209}$Bi, where evaporation of one neutron ($1n$) from the compound nucleus results in ^{212}At as well. We do not present the results for the ^{211}Po compound nucleus formed by ICF of $d + ^{209}$Bi, since a calibration reaction is not available for comparison.

(ii) The nucleus ^{7}Li may break up into an α particle and a triton ($S_\alpha = 2.45$ MeV), forming the ICF products ^{212}At and ^{211}Po, respectively, following evaporation of $1n$ from the compound nucleus. The results for ^{211}Po are given in the Appendix, since a calibration reaction with a t beam is not available. The same products are formed through the calibration reactions of $\alpha + ^{209}$Bi and $\alpha + ^{208}$Pb, after one-neutron evaporation from the compound nucleus.

(iii) Capture of one of the breakup fragments of ^{9}Be (^{8}Be + $n \rightarrow ^4$He $+ ^4$He $+ n$; $S_n = 1.67$ MeV or ^{5}He $+ ^4$He; $S_\alpha = 2.55$ MeV) by ^{208}Pb forms the residue ^{211}Po after $1n/2n$ evaporation from the compound nucleus. This nucleus is also formed as an evaporation residue in the calibration reaction $\alpha + ^{208}$Pb after $1n$ evaporation.

III. THE EXPERIMENTAL METHOD

The CF and ICF measurements for the ^{6}Li + ^{209}Bi, ^{7}Li + ^{209}Bi, and ^{9}Be + ^{208}Pb reactions were carried out using the 14 UD tandem accelerator at the Australian National University. Most of the measurements were done with pulsed beams, with laboratory energies ranging from 26.0 to 52.0 MeV. The experimental method is described in detail in Refs. [14–16] and only a brief description is given here. Beams of ^{6}Li, ^{7}Li, and ^{9}Be were incident on self-supporting ^{nat}Bi and enriched ($>99\%$) ^{208}PbS targets evaporated onto 15 μg/cm^2 C foils. Recoiling evaporation residues were stopped in aluminium catcher foils placed immediately behind the targets. The α particles from short-lived ($T_{1/2} \leqslant 24$ min) CF and ICF products were detected by an annular Si surface-barrier detector. Two Si surface-barrier detectors (monitors), symmetrically placed about the beam axis at forward angles, were used to measure the elastically scattered beam particles, for normalization purposes. Absolute cross sections were determined by measuring sub-barrier elastic scattering in the annular detector and monitors. Since the energies of the α particles emitted by the isomeric state and ground state for both ^{211}Po and ^{212}At nuclei differ by a few hundred keV, the population of the isomer and the ground state can be determined separately. Thus, the number of α particles from each state represents an excellent measure of the number of nuclei populated in each level. For illustration, typical α-particle energy spectra for the ^{6}Li + ^{209}Bi and ^{9}Be + ^{208}Pb reactions collected during irradiation are shown in Fig. 1. All
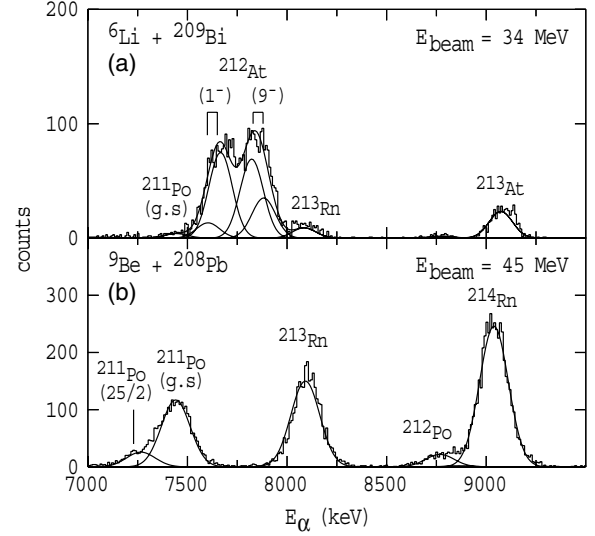

FIG. 1. Typical measured α spectra collected during irradiation for (a) the ^{6}Li + ^{209}Bi reaction at a beam energy of 34 MeV and (b) the ^{9}Be + ^{208}Pb reaction at a beam energy of 45 MeV. The lines are fits to the α spectrum.

the peaks can be clearly identified. The measured ICF cross sections for the ^{212}At and ^{211}Po ground state and isomeric state are given in Tables I–III.

IV. ISOMER RATIO CALIBRATION

The calculation of the isomer ratio for a particular reaction, in principle, needs two ingredients: (i) the angular momentum distribution of the compound nucleus and (ii) the feeding from the compound states to the isomer and ground states. According to Bohr's compound-nucleus model, the latter should be independent of the reaction forming the compound system.

TABLE I. Ground-state and isomeric-state cross sections for ^{212}At formed following incomplete fusion of ^{6}Li with ^{209}Bi. The $E_{\rm c.m.}$ is corrected for energy losses in the target.

$E_{\rm beam}$ (MeV)	$E_{\rm c.m.}$ (MeV)	^{212}At (1^-) (mb)	^{212}At (9^-) (mb)
28.00	27.11	0.94 ± 0.14	0.46 ± 0.09
29.00	28.06	2.32 ± 0.20	1.24 ± 0.14
30.00	29.08	5.1 ± 0.3	2.98 ± 0.24
31.00	30.04	8.7 ± 0.4	5.6 ± 0.3
32.00	30.98	11.9 ± 0.5	9.9 ± 0.5
33.00	32.00	14.9 ± 0.8	14.3 ± 0.6
34.00	32.96	16.6 ± 0.6	19.6 ± 0.7
36.00	34.92	17.3 ± 0.6	28.9 ± 0.8
38.00	36.86	16.3 ± 0.6	35.5 ± 0.9
40.00	38.81	14.6 ± 0.2	39.5 ± 1.2
44.00	42.70	10.4 ± 0.5	35.1 ± 1.0
48.00	46.58	6.6 ± 0.5	27.6 ± 0.9

TABLE II. Ground-state and isomeric-state cross sections for ^{212}At and ^{211}Po evaporation residues formed following incomplete fusion of ^{7}Li with ^{209}Bi. The $E_{c.m.}$ is corrected for energy losses in the target.

E_{beam} (MeV)	$E_{c.m.}$ (MeV)	^{212}At (1^-) (mb)	^{212}At (9^-) (mb)	^{211}Po $(9/2^+)$ (mb)	^{211}Po $(25/2^+)$ (mb)
26.00	25.02			1.58 ± 0.18	
27.00	26.01			3.84 ± 0.25	
28.00	26.98			8.6 ± 0.4	0.46 ± 0.09
29.00	27.95	0.73 ± 0.10	0.33 ± 0.08	13.9 ± 0.5	1.30 ± 0.11
30.00	28.92	2.20 ± 0.18	1.04 ± 0.15	20.3 ± 0.6	2.62 ± 0.17
31.00	29.89	4.53 ± 0.30	2.59 ± 0.27	25.0 ± 0.8	3.68 ± 0.23
32.00	30.86	6.9 ± 0.4	4.50 ± 0.35	28.7 ± 0.9	6.3 ± 0.3
33.00	31.77			30.4 ± 1.0	6.0 ± 0.4
33.00	31.83	9.1 ± 0.5	8.1 ± 0.5	31.8 ± 1.3	6.0 ± 0.3
34.00	32.80	11.6 ± 0.5	10.1 ± 0.6	32.2 ± 1.1	7.0 ± 0.4
35.00	33.70			31.6 ± 1.1	8.3 ± 0.6
35.00	33.77	11.7 ± 0.5	12.5 ± 0.6	31.4 ± 1.6	6.2 ± 0.5
36.00	34.70	11.2 ± 0.8	13.3 ± 1.0	30.3 ± 1.5	6.8 ± 0.6
37.00	35.50			31.4 ± 1.7	4.2 ± 0.6
38.02	36.68	11.0 ± 0.8	14.4 ± 1.1	28.3 ± 1.6	5.7 ± 0.6
39.00	37.59			25.8 ± 2.1	3.18 ± 0.69
40.00	38.63	9.2 ± 0.6	18.4 ± 1.0	26.3 ± 1.2	5.4 ± 0.4
44.00	42.53	7.6 ± 0.7	23.9 ± 1.4	19.3 ± 1.3	4.5 ± 0.7
48.00	46.34	8.4 ± 0.6	35.5 ± 1.4	17.1 ± 1.0	5.1 ± 0.5
52.00	50.23	5.6 ± 0.4	41.9 ± 1.3	14.9 ± 0.8	4.7 ± 0.3

To calculate the angular momentum distribution of the compound nucleus it is necessary to reproduce [20] the experimental fusion excitation function of the corresponding reaction. For all the cases considered in this work, the CCFULL code [21] was used to carry out a coupled-channel analysis to fit the measured total fusion (CF + ICF) cross sections. The parameters that define the real Woods-Saxon nuclear potential used in the coupled-channel calculations are presented in Table IV. For the calibration reactions the agreement between the data and the theoretical results is excellent in the energy

region of interest. For the reactions involving weakly bound projectiles the experimental fusion data are well described by the CCFULL calculations. A detailed discussion of the quality of the fits can be found in Ref. [16]. Since the projectile and target have nonzero spin, the total angular momentum distribution was obtained by folding the orbital angular momentum with the intrinsic spins. Once the angular momentum distribution of the compound nucleus is determined, the next step requires a complete knowledge of the decay paths to the yrast line and states around the yrast line. Because this information is not available, we take a phenomenological approach in this work. The population of the isomeric state compared to the ground state is calculated by splitting the angular momentum distribution of the compound nucleus into two regions. The lower angular momentum region feeds the ground state; the higher feeds the isomer. The simplest approach would be to apply a sharp cutoff at the angular momentum of the isomer. However, because of neutron evaporation and the cascade of γ rays from the compound nucleus, a spread in the angular momentum distribution is expected. Furthermore, these effects

TABLE III. Ground-state and isomeric-state cross sections for the ^{211}Po nucleus formed following incomplete fusion of ^{9}Be with ^{208}Pb. The $E_{c.m.}$ is corrected for energy losses in the target.

E_{beam} (MeV)	$E_{c.m.}$ (MeV)	^{211}Po $(9/2^+)$ (mb)	^{211}Po $(25/2^+)$ (mb)
36.00	34.40	0.65 ± 0.31	
37.00	35.37	1.03 ± 0.59	
38.00	36.33	7.9 ± 1.2	0.31 ± 0.12
39.00	37.29	19.0 ± 1.8	1.77 ± 0.33
40.00	38.25	32.5 ± 2.3	3.13 ± 0.86
41.02	39.22	50.7 ± 2.5	6.7 ± 0.6
42.00	40.16	62.5 ± 3.1	10.2 ± 0.8
43.00	41.12	80.3 ± 3.9	12.7 ± 1.2
44.06	42.15	96.6 ± 3.4	17.8 ± 1.4
45.00	43.05	106.8 ± 4.0	24.4 ± 2.0
46.00	44.01	106.8 ± 4.0	36.0 ± 2.8
47.00	44.96	101.0 ± 3.8	43.0 ± 3.0
48.00	45.92	96.0 ± 3.8	51.2 ± 3.6
49.00	46.88	93.5 ± 3.9	56.5 ± 3.4
50.00	47.84	94.6 ± 3.8	51.7 ± 3.2
51.00	48.80	87.3 ± 4.1	57.8 ± 3.4

TABLE IV. The Woods-Saxon nuclear potential parameters used in the coupled-channel calculations. V_0 is the potential depth, R_0 is the nuclear radius, and a is the diffuseness.

System	V_0 (MeV)	R_0 (fm)	a (fm)
^{4}He + ^{208}Pb	87	7.89	0.70
^{4}He + ^{209}Bi	77	7.90	0.70
^{6}Li + ^{209}Bi	89	8.68	0.63
^{7}Li + ^{209}Bi	95	8.79	0.63
^{9}Be + ^{208}Pb	134	8.81	0.63

in general will also result in the angular momentum at the yrast line being different from that of the compound nucleus. To account for these features empirically, we calculate the isomer ratio R, using an effective angular momentum cutoff J_{eff}, and a spreading parameter δ:

$$R = \frac{\sum_J \sigma_J^{(2)}}{\sum_J \sigma_J^{(1)}}, \tag{1}$$

$$\sigma_J^{(1)} = \frac{\sigma_J}{1 + \exp\left(\frac{J_{\text{eff}} - J}{\delta}\right)}, \tag{2}$$

$$\sigma_J^{(2)} = \frac{\sigma_J}{1 + \exp\left(\frac{J - J_{\text{eff}}}{\delta}\right)}, \tag{3}$$

where the σ_J correspond to the total angular momentum distribution for a particular compound nucleus and $\sigma_J^{(1)}$ ($\sigma_J^{(2)}$) represents the angular momentum distributions associated with the ground state (isomeric state). The value of the spreading parameter δ in the Fermi function determines the extent of smoothing around J_{eff}. We assumed $\delta = 0.5$ in our calculations, which may be reasonable to account for the angular momentum carried by the neutrons and γ rays. The consequences of adopting a larger value of δ are very minor, as will be discussed in Sec. V C. A schematic picture depicting this procedure is shown in Fig. 2 for the ^{6}Li + ^{209}Bi angular momentum distribution calculated at $E_{\text{c.m.}} = 35$ MeV. Note that this method can only be applied to nuclei that have no other isomeric state competing with the one of interest.

Before applying the phenomenological approach to study the breakup reactions, it is necessary to reproduce the isomer ratios for the calibration reactions $\alpha + ^{209}$Bi and $\alpha + ^{208}$Pb [18,19]. As a starting point, J_{eff} was set to be equal to the angular momentum of the isomeric state of the corresponding products ^{212}At and ^{211}Po. In this simple description we are assuming that all nuclei populated at an angular momentum
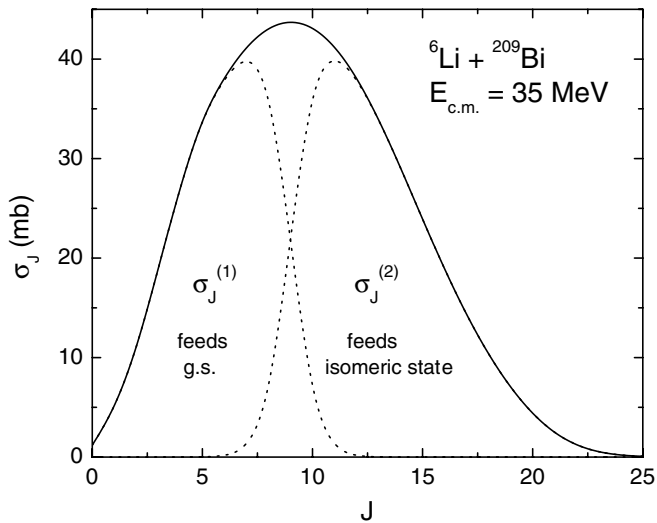

FIG. 2. The solid line corresponds to the angular momentum distribution for the total fusion of ^{6}Li + ^{209}Bi calculated at $E_{\text{c.m.}} = 35$ MeV. The division of population between the ground state and the isomeric state in the phenomenological approach is indicated by the dotted lines, for $\delta = 0.5$ and $J_{\text{eff}} = 9$.
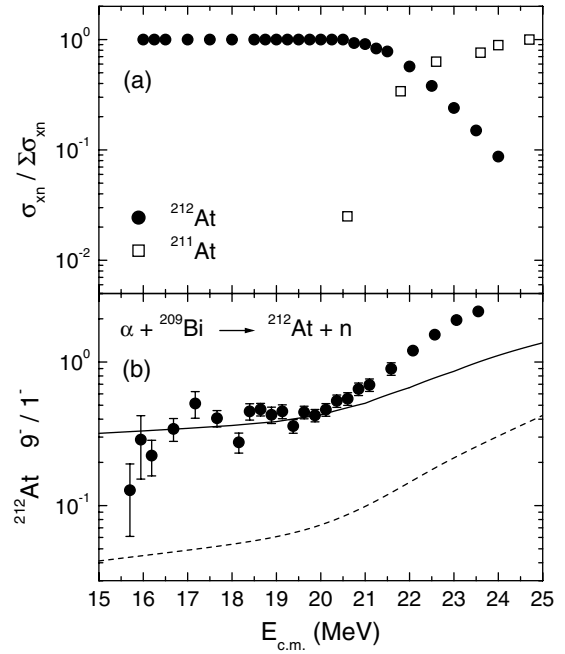

FIG. 3. (a) The ratio of the yields of specific xn evaporation channels to the total xn cross section for the $\alpha + ^{209}$Bi reaction. (b) The measured [16] and predicted isomer ratio for ^{212}At formed through the $\alpha + ^{209}$Bi reaction as a function of c.m. energy. The dashed line corresponds to the calculation using $J_{\text{eff}} = 9$ and the solid line refers to the calculation using $J_{\text{eff}} = 6.4$. The predictions do not match the data at $E_{\text{c.m.}} > 22$ MeV, where the $2n$ evaporation channel becomes dominant (see text for details).

higher than the isomer will feed the isomeric state whereas nuclei populated with angular momentum lower than the isomer will populate the ground state. Using Eqs. (1)–(3) and $J_{\text{eff}} = 9$, we show the isomer ratios for $\alpha + ^{209}$Bi in Fig. 3(b) by the dashed line. The result for $\alpha + ^{208}$Pb obtained with $J_{\text{eff}} = (25/2)$ is represented by the dashed line in Fig. 4. Despite the calculations having the same slope as the data, they are roughly one order of magnitude lower. This implies that the isomeric state is more highly populated than is predicted by the empirical calculations. States that are populated in fusion with angular momentum lower than the isomer apparently have some probability of decaying to higher angular momentum states. In the present work we empirically account for this effect by considering J_{eff} as an adjustable parameter determined from the best fit to the corresponding experimental isomer ratio. In the ^{212}At case $J_{\text{eff}} = 6.4$ provides the best description for the measured isomer ratio, whereas for the ^{211}Po case $J_{\text{eff}} = 10$. The resulting calculations are shown by solid lines in Figs. 3(b) and 4. Because of the increasing slope of the yrast line with angular momentum, angular momentum fractionation between xn channels will occur; xn channels with fewer than average neutrons are associated with the higher partial waves. As shown in Fig. 3(a), the $1n$ evaporation channel dominates the fusion excitation function in the near-barrier energy region ($V_B = 20$ MeV). The evaporation of two neutrons becomes the dominant part of the total fusion cross section at energies beyond 22 MeV and our phenomenological approach will predict too low
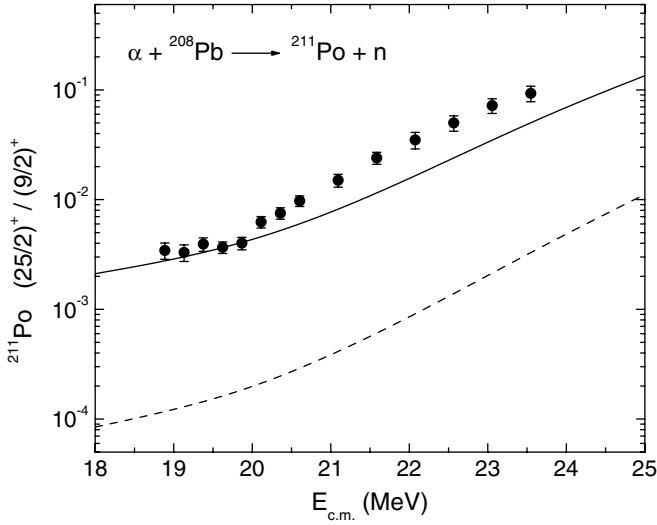
FIG. 4. Same as lower panel of Fig. 3 but for ^{211}Po formed in the $\alpha + {}^{208}$Pb fusion reaction. The calculations using $J_{\text{eff}} = (25/2)$ (dashed line) and $J_{\text{eff}} = 10$ (solid line) are presented in the figure.

an isomer ratio. For the $\alpha + {}^{208}$Pb reaction only the $1n$ evaporation cross section data are available. Considering the similarity between the two reactions, their experimental isomer ratios are well described by the present phenomenological approach in the energy range where the $1n$ evaporation channel dominates.

V. INCOMPLETE FUSION REACTIONS

Having determined empirically J_{eff} for the ^{212}At and ^{211}Po nuclei, the breakup mechanism of ^{6,7}Li and ^{9}Be incident on targets of ^{208}Pb and ^{209}Bi, which form the same nuclei, may be investigated via the measured ICF isomer ratio. It is assumed that the angular momentum carried after breakup by the part of the projectile that is captured by the target is proportional to the ratio of the mass of the fragment divided by the mass of the projectile. Thus, the angular momentum distribution corresponding to the ICF reaction can be defined as the product of the total (CF + ICF) angular momentum distribution and the ratio between the mass of fragment and projectile. To partition the angular momentum distribution into CF and ICF contributions to the total fusion cross section, two extreme assumptions [22] will be made. The first and simplest assumption is that all partial waves contribute to ICF with the same probability. The second is that only the higher partial waves lead to ICF. Both approaches are employed to interpret the ^{211}Po and ^{212}At isomer ratio data related to the $\alpha + {}^{208}$Pb and $\alpha + {}^{209}$Bi ICF reactions following breakup. The results are presented in the following.

A. All angular momenta

In this scenario, the effective isomer angular momentum values J_{eff} for the products ^{212}At and ^{211}Po determined from the calibration reactions are used to split the ICF angular momentum distribution into ground-state and isomeric-state
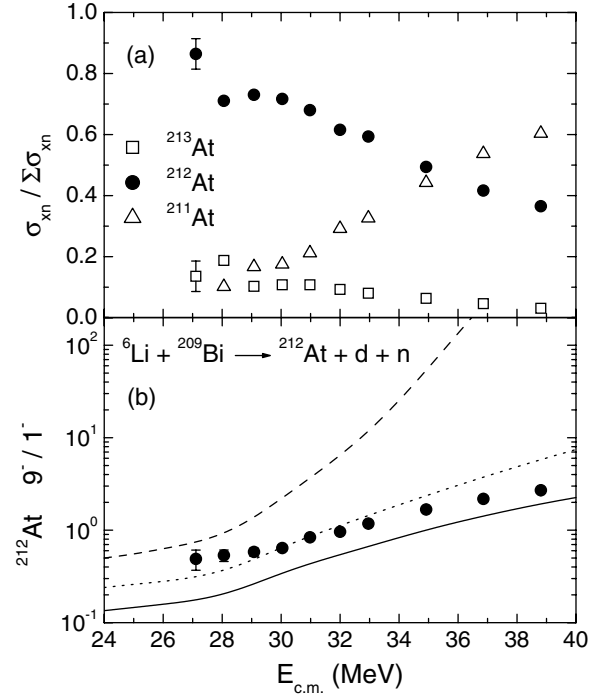

FIG. 5. (a) The ratio of the xn evaporation channel to the total xn cross section for the ^{6}Li $+ {}^{209}$Bi ICF reaction. (b) The solid (dashed) line represents the results obtained with the all-angular-momenta (high-angular-momenta) approximation with $J_{\text{eff}} = 6.4$. The dotted line is obtained using the high-angular-momenta approximation with $\Delta = 5$ (see text for details).

regions, as shown in Fig. 2. Figures 5(b) and 6(b) show the calculated ^{212}At isomer ratio (solid line) compared with the experimental data obtained from the ^{6,7}Li $+ {}^{209}$Bi reactions, respectively. The calculation underestimates the data by a factor of approximately 3 in the region where the $1n$ evaporation is predominant [see Figs. 5(a) and 6(a)]. This result indicates that the contribution of the higher partial waves should be larger. For the ^{211}Po isomer ratio in the ^{9}Be $+ {}^{208}$Pb reaction the calculations underpredict the data for the the entire range of energy and are about two orders of magnitude smaller than the measured data for the lowest energy, as indicated by the solid line in Fig. 7(b). This may be because J_{eff} is larger for ^{211}Po as compared to ^{212}At and hence the isomer ratio is more sensitive to the higher angular momentum component brought in. As can clearly be seen, the all-angular-momenta approximation fails to describe the isomer ratio data for the $\alpha + {}^{208}$Pb and $\alpha + {}^{209}$Bi ICF reactions. A larger population of the isomer is required in all reactions.

B. High angular momenta

In this approach, only the higher angular momenta contribute to the ICF reactions, with the CF associated exclusively with the remaining lower partial waves. Table V shows the measured percentage of the total fusion cross section resulting in CF and ICF for the reactions ^{6}Li $+ {}^{209}$Bi, ^{7}Li $+ {}^{209}$Bi, and ^{9}Be $+ {}^{208}$Pb [14–16]. A partial wave value is determined,

TABLE V. The proportion of the total fusion cross section resulting in CF and ICF for the reactions ^{6}Li + ^{209}Bi, ^{7}Li + ^{209}Bi, and ^{9}Be + ^{208}Pb, from Ref. [16].

System	CF (%)	ICF (%)
^{6}Li + ^{209}Bi	66	34
^{7}Li + ^{209}Bi	71	29
^{9}Be + ^{208}Pb	68	32

dividing the total angular momentum distribution into CF and ICF parts, in accordance with the fraction of the total fusion corresponding to the ICF process (see Table V). We used a Fermi function with a diffuseness Δ equal to 0.5 to allow the cutoff to be smooth. To illustrate this procedure, in Fig. 8 we show the calculated angular momentum distribution of the ICF for the ^{6}Li + ^{209}Bi reaction at $E_{c.m.} = 35$ MeV by the vertical hatched region. The solid line indicates the angular momentum distribution corresponding to the total fusion cross section (CF + ICF). This was the one used in the previous calculations by adopting the all-angular-momenta approach.

By using the effective isomer angular momentum values J_{eff} determined from the calibration reactions in Sec. IV for the products ^{212}At and ^{211}Po, the isomer ratio for the reactions ^{6}Li + ^{209}Bi, ^{7}Li + ^{209}Bi, and ^{9}Be + ^{208}Pb were calculated. The results for ^{212}At are presented as dashed line in the lower panels of Figs. 5 and 6. In contrast to the results obtained by using the all-angular-momenta approach, the high-angular-momenta approximation overestimates the measured isomer ratio in the entire range of energy. Clearly, the low partial waves also contribute to ICF and cannot only be associated with the CF process. To verify this statement we assume a larger value for
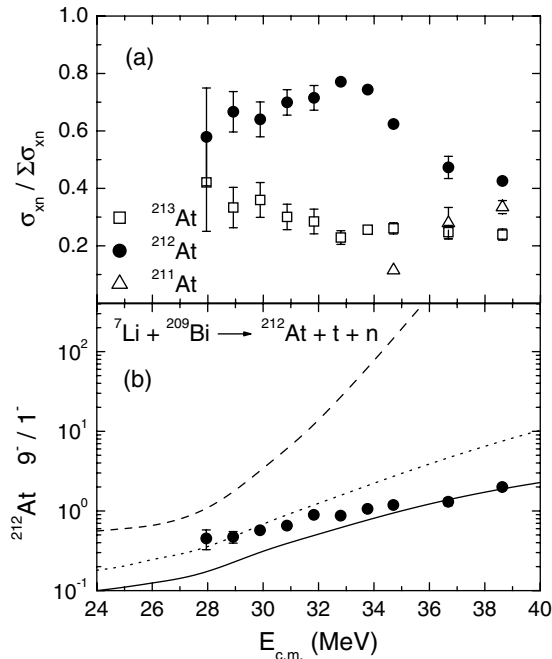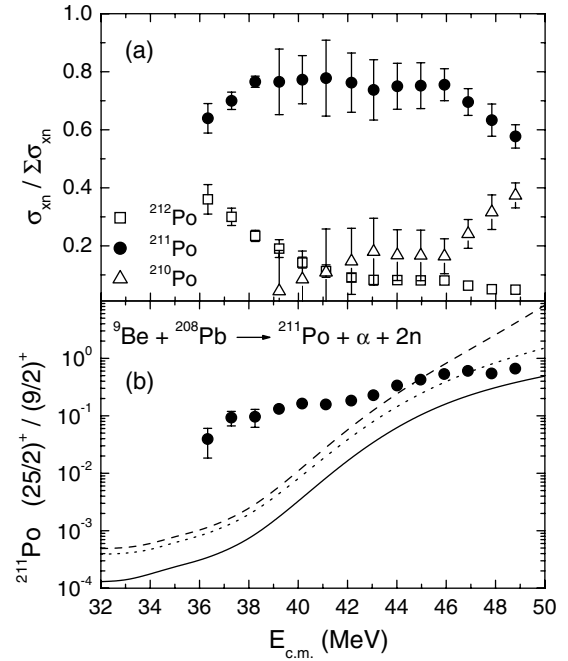

FIG. 7. Same as Fig. 5 but for the ^{211}Po nucleus formed in the ^{9}Be + ^{208}Pb ICF reaction.

the diffuseness parameter Δ in the Fermi function that divides the angular momentum distribution into CF and ICF regions (see the horizontal hatched region in Fig. 8). By comparing the dotted and dashed lines in Figs. 5(b) and 6(b), the agreement between data and theoretical prediction is greatly improved when the diffuseness is ten times larger (i.e., $\Delta = 5$). This
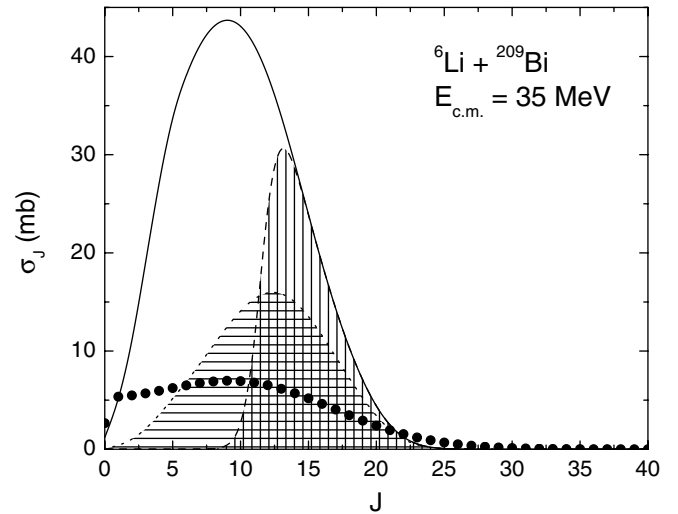

FIG. 6. Same as Fig. 5 but for the ^{7}Li + ^{209}Bi ICF reaction.

FIG. 8. Angular momentum distribution for the ^{6}Li + ^{209}Bi reaction at $E_{c.m.} = 35$ MeV. The solid line shows the total fusion (CF + ICF). For the assumption that the higher partial waves result exclusively in ICF, the vertical hatched region corresponds to ICF for $\Delta = 0.5$; the horizontal hatched region is obtained with $\Delta = 5.0$ (see Sec. V B for details). The circles are obtained by including spreading in the angular momentum distribution brought into the system by the ICF fragments required to reproduce the experimental isomer ratio data (see Sec. V C for details).

result indicates that neither the all-angular-momenta nor the high-angular-momenta approach is appropriate to describe the isomer ratio data. For ^{212}At formed in ICF with ^{6,7}Li, it appears that a condition between the two extreme approximations can describe the measured isomer ratios. However, for ^{211}Po, having an isomer at higher angular momentum, the situation is very different. The results obtained with the high-angular-momenta approximation [dashed line in Fig. 7(b)] are closer to the data than the results obtained with the all-angular-momenta approximation. Nevertheless, the overall agreement between the calculations and experimental results is still unsatisfactory. In this case, since both approaches underpredict the measured isomer ratios at the lower beam energies, there is no better agreement between the calculations and data by assuming a larger value of diffuseness Δ in the Fermi function that divides the CF and ICF contributions in the total angular momentum distribution, as indicated by the dotted line in Fig. 7(b).

The ^{211}Po isomer ratio, sampling the higher partial waves, indicates that angular momenta are populated beyond those predicted by the simple scaling procedure adopted in Sec. V A and V B.

C. Angular momentum spread

During the breakup process the energy of the projectile is assumed to be shared between the fragments in proportion to their masses. Since the fragments are charged, they will experience a mutual Coulomb repulsion that will result in a distribution of energies as well as modifying the point of interaction (impact parameter) with the target nucleus.

To account for these effects in a simple manner the cross section of each partial wave is folded with a Gaussian distribution. The standard deviation of the Gaussian distribution, σ, represents a free parameter, and it is adjusted to describe the experimental isomer ratio for each reaction. An example of this folded angular momentum distribution is shown by the filled circles in Fig. 8 for the ^{6}Li + ^{209}Bi reaction at $E_{c.m.} = 35$ MeV. As our main goal in this work is to provide a global description of the experimental isomer ratio, we assume that σ does not vary as a function of angular momentum and energy for a particular reaction. Also, we should not expect that one universal value of σ could describe the measured isomer ratio for all reactions since the breakup mechanism should be system dependent. However, as shown in Table VI, for the all-angular-momenta limit the values of σ only differ slightly.

TABLE VI. The values of σ used for folding each partial wave (see text) that corresponds to the best fit of the measured isomer ratio for each breakup reaction.

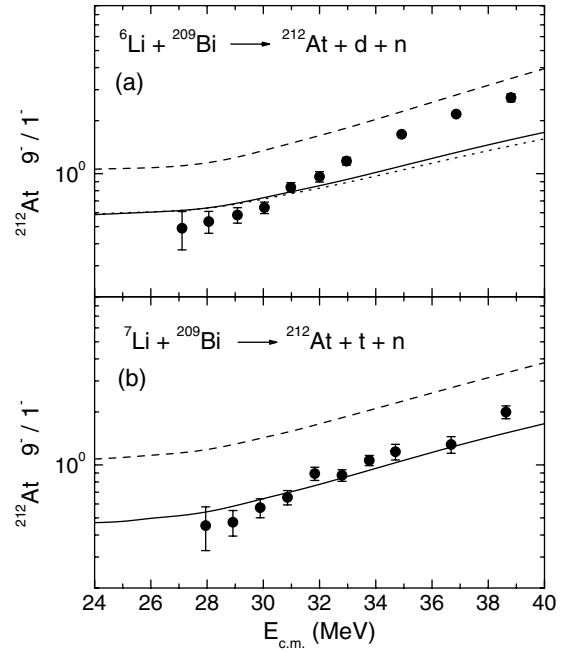| System	Product	σ_{all}	σ_{high}
^{6}Li + ^{209}Bi	^{212}At	5.4	6.9
^{7}Li + ^{209}Bi	^{212}At	4.7	7.4
^{9}Be + ^{208}Pb	^{211}Po	4.7	3.2
^{7}Li + ^{209}Bi	^{211}Po	5.0	3.0

FIG. 9. (a) The measured isomer ratio for ^{212}At formed in the ^{6}Li + ^{209}Bi reaction. The solid (dotted) line represents the results obtained with the all-angular-momenta approximation with $\delta = 0.5$ (1.0) and includes the angular momentum spreading by adopting $\sigma = 5.4$. The dashed line refers to the calculations using the high-angular-momenta approach and $\sigma = 6.9$. (b) Same as (a) but for the ^{7}Li + ^{209}Bi reaction. The solid (dashed) line is obtained with the all-angular-momenta (high-angular-momenta) approximation and $\sigma = 4.7$ (7.4).

The solid line in Fig. 9(a) shows the results of calculations by assuming the all-angular-momenta approach and $\sigma = 5.4$. The agreement between data and calculations for ^{212}At, derived from the ^{6}Li + ^{209}Bi reaction, can be considered satisfactory for the energy range where the $1n$ evaporation channel dominates. For the ^{7}Li + ^{209}Bi reaction, the results for the ^{212}At isomer ratio are well described by the all-angular-momenta approach with $\sigma = 4.7$, as shown by the solid line in Fig. 9(b). For the ^{6,7}Li-induced reactions, the high-angular-momentum approximation already overpredicts the isomer ratio. Adding angular momentum spreading (e.g., with $\sigma = 6.9$ and $\sigma = 7.4$ in Figs. 9(a) and 9(b), dashed lines, respectively) can minimize the overall disagreement, but no value of σ gives a good description of the data.

To verify the dependence of our simple approach on the Fermi function that smooths the sharp cutoff at J_{eff} (2) and (3) we calculate the ^{212}At isomer ratio (^{6}Li + ^{209}Bi) by adopting the all-angular-momenta approach with $\delta = 1.0$. In Fig. 9(a) we compare this result (dotted line) with the isomer ratios obtained by assuming $\delta = 0.5$ (solid line). $\delta = 1.0$ requires $J_{eff} = 6.7$ and $\sigma = 5.7$ to better describe the experimental isomer ratio. Clearly, increasing δ by a factor of 2 hardly affects the overall agreement between data and theoretical results.

For ^{9}Be + ^{208}Pb, probed by the ^{211}Po isomer ratio, $\sigma = 4.7$ gave the best agreement with the measured isomer ratio using the all-angular-momenta approximation, as indicated by the solid line in Fig. 10. The dashed line
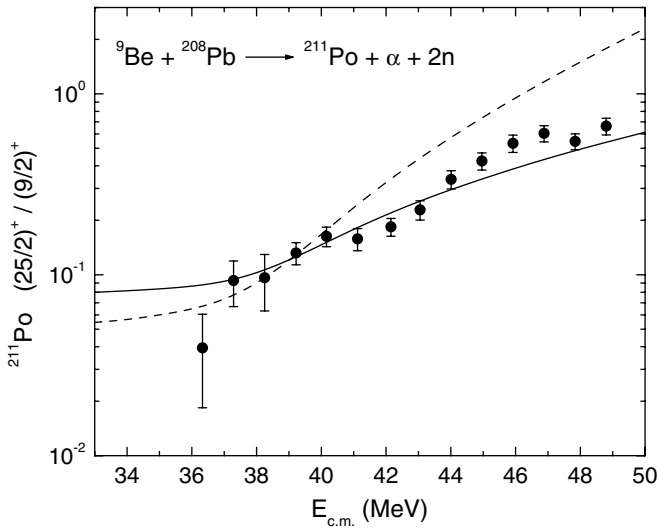
FIG. 10. Same as Fig. 9 but for the ^{9}Be $+$ ^{208}Pb reaction. The solid (dashed) line represents the calculation using the all-angular-momenta (high-angular-momenta) approximation with $\sigma =$ 4.7 (3.2).

in Fig. 10 represents the results obtained by assuming the high-angular-momenta approach with $\sigma = 3.2$. The empirical spreading in the angular momentum (which can result from the mutual Coulomb interaction between the fragments of the projectile) greatly affects the isomer ratio prediction. In general, the all-angular-momenta approach provides a better overall description of the isomer ratio data in comparison with the high-angular-momenta limit. Obviously, a more detailed kinematic calculation is required to quantitatively describe the breakup mechanism.

VI. CLASSICAL THREE-BODY KINEMATICAL CALCULATION

The fact that the breakup mechanism has a significant effect on the angular momentum brought into the system by the fragments during the ICF process is confirmed by realistic calculations based on a 3D classical trajectory model [23]. In this approach the breakup of the projectile is encoded by assuming a local breakup probability as a function of the projectile-target separation, termed the breakup function. This function has the same form as the integrated breakup probability over the whole trajectory, which is found to be an exponential function of the minimal projectile-target separation in experiments of ^{9}Be $+$ ^{208}Pb at sub-barrier energies [24]. The breakup function is used to sample the breakup radius along with the breakup probability, with a range of initial conditions (excited state of the projectile, separation between the breakup fragments, and orientation of the fragments) by using the Monte Carlo method. The breakup fragments are assumed to be isotropically oriented in the projectile center of mass. The projectile-target orbit before the breakup is matched to that of the post-breakup fragments by conservation of energy, linear momentum, and angular momentum in the overall c.m. frame of the projectile and

target system. Further details of the model will be published in a forthcoming paper [23].

The interaction between the 2α plus neutron after ^{9}Be breakup with the ^{208}Pb target represents a very complex four-body problem. For the sake of simplicity, calculations were performed for the reaction ^{8}Be $+$ ^{208}Pb, with a laboratory incident energy of 45 MeV. An ICF event occurs when one α particle penetrates the radius of the α-^{208}Pb s-wave Coulomb barrier. The ICF cross sections are calculated with the classical sharp cutoff formula and all ^{8}Be partial waves leading to ICF have been taken into account in the calculations. A sample of 1000 breakup events is used for each ^{8}Be partial wave.

The angular momentum distribution brought into the compound nucleus for the case where ^{212}Po is formed by absorption of one α particle by the ^{208}Pb target in the breakup reaction is shown by the circles in Fig. 11(a). The vertical hatched lines in Fig. 11(a) show the angular momentum distribution of ^{212}Po formed in CF of a direct beam of 22.5 MeV α-particles impinging on ^{208}Pb (equivalent to $E_{\text{Lab}}^{^8\text{Be}} = 45$ MeV); the maximum partial wave leading to fusion is 6. Comparison with the circles shows that the breakup process can increase the angular momentum of the compound system formed by
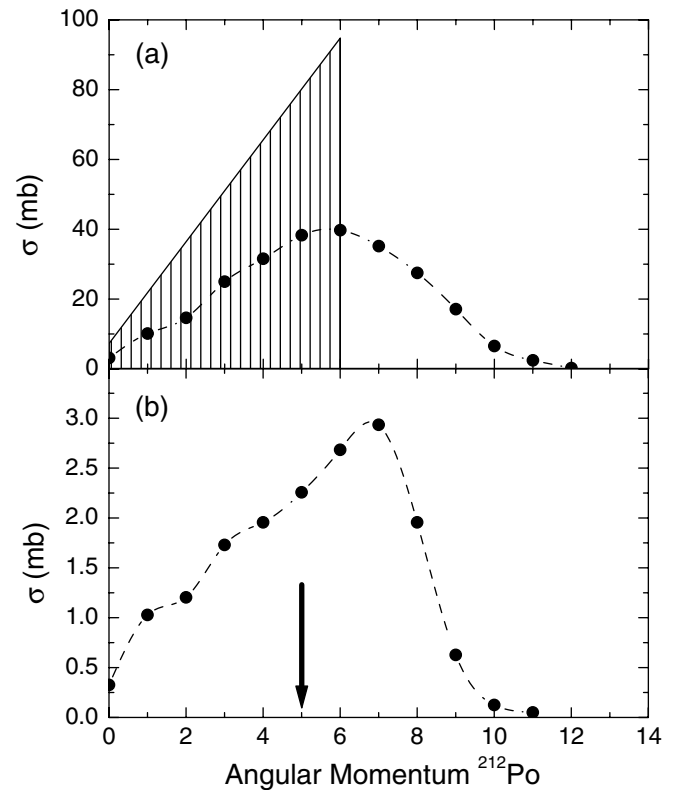

FIG. 11. (a) Calculated partial cross sections σ_ℓ for ^{212}Po when formed by (i) fusion of an α particle following breakup of 45-MeV ^{8}Be incident on ^{208}Pb (circles) and (ii) fusion of a direct beam of 22.5 MeV α-particles with ^{208}Pb (vertical hatched area). (b) Partial cross sections for ^{212}Po formation showing the spread in angular momentum brought in by the breakup α particle from a ^{8}Be projectile with a fixed angular momentum of 10. The thick arrow indicates the maximum angular momentum for fusion of $\alpha + {}^{208}$Pb if ^{8}Be is considered to be a pointlike object.

ICF well beyond the maximum value when only the captured fragment interacts with the target. The ICF cross sections corresponding to a fixed orbital angular momentum of the incident projectile ^{8}Be ($\ell_{proj} = 10$) is shown as circles in Fig. 11(b). If ^{8}Be is considered to be a pointlike object, an α particle carries half of the ^{8}Be incident angular momentum, as denoted by the thick arrow in Fig. 11(b). Clearly, a spreading of the angular momentum brought into the target by an α particle occurs following breakup of the ^{8}Be projectile.

VII. SUMMARY AND CONCLUSIONS

In this work, isomer ratios in ICF reactions were studied. The main goal here is to investigate the effect of the breakup on the angular momentum distribution brought into the compound nucleus formed following ICF. The parameters of a simple phenomenological picture were adjusted to reproduce the measured isomer ratios in residues formed by fusion reactions with α beams leading to the same nuclei as produced in ICF. By adopting an effective isomer angular momentum value J_{eff} to divide the population between the ground state and the isomeric state, the experimental ^{211}Po and ^{212}At isomer ratios for the calibration reactions $\alpha + ^{208}$Pb and $\alpha + ^{209}$Bi were reproduced. Under the assumption that ICF occurs with equal probability for all partial waves, insufficient angular momentum is introduced to explain the isomer ratios measured in ICF reactions. Within a simple phenomenological approach, assuming that only the highest partial waves lead to ICF still leads to lower predicted isomer ratios than those measured for ^{211}Po. Only by introducing additional spreading of the angular momentum distribution, which is likely to be due to the interaction between the projectile fragments, can the measurements be reproduced. This result gives strong evidence that the breakup dynamics has a significant effect on the angular momentum brought into the system by the fragments during the ICF process. Thus, a quantitative understanding of the ICF process requires a theoretical model that follows the projectile fragments trajectories up to their end point. Initial results obtained with a 3D classical trajectory model indicate that the angular momentum brought into the system by the α particle after breakup for the reaction ^{8}Be + ^{208}Pb can exceed the angular momentum that would be brought into the system by using an α beam incident on a ^{208}Pb target. The isomer ratio data are very sensitive to the input angular momentum distributions, as indicated by the results obtained by using the two limiting angular momentum partition assumptions made in this work. Therefore, isomer ratio measurements could be used to test and develop future realistic models of breakup and fusion.

APPENDIX: $t + ^{209}$BI INCOMPLETE FUSION REACTION

^{7}Li can break up into an α particle and a triton, with the latter forming the ICF product ^{211}Po after evaporation of one neutron from the compound nucleus. Although data corresponding to the triton calibration reaction are not available, we calculate the ^{211}Po isomer ratio for the ICF $t + ^{209}$Bi reaction by assuming the same effective isomer angular momentum value as obtained using the $\alpha + ^{208}$Pb calibration reaction ($J_{eff} = 10$) to divide the population between the ground state and the isomeric state. The results are shown in the lower panel of Fig. 12 by the solid and dashed lines. The behavior is similar to the ^{211}Po isomer ratio obtained from the ^{9}Be + ^{208}Pb reaction; both all-angular-momenta and high-angular-momenta approximations underpredict the experimental isomer ratio for most data points available. The upper panel of Fig. 12 presents the ratio of the yield of the $0n$ (open triangles), $1n$ (close circles), and $2n$ (open squares) evaporation channels to the total xn cross section for the ICF $t + ^{209}$Bi reaction. The ^{210}Po product dominates the entire range of energy. Since $2n$ evaporation is the dominant channel here, the $\alpha + ^{208}$Pb $\rightarrow ^{211}$Po $+ n$ reaction should not be strictly applicable as a calibration reaction (in lieu of $t + ^{209}$Bi) because the angular momentum fractionation between the $1n$ and $2n$ channels can change J_{eff}. However, for ^{211}Po to be dominant in the ^{7}Li reaction, the
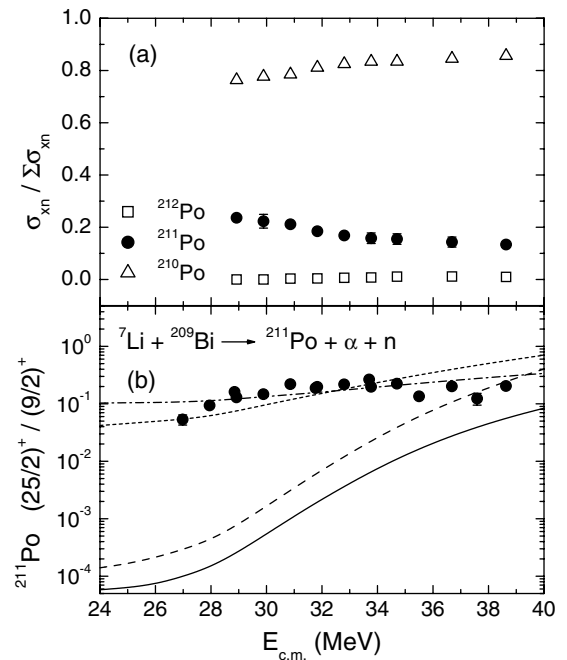

FIG. 12. (a) The ratio of the yield of the xn evaporation channel to the total xn cross section corresponding to capture of the lighter fragment following breakup in the ^{7}Li + ^{209}Bi reaction. (b) The measured and predicted isomer ratio for ^{211}Po formed through the $t + ^{209}$Bi reaction as a function of c.m. energy. The solid (dashed) line represents the results obtained with the all-angular-momenta (high-angular-momenta) approximation with $J_{eff} = 10$. The dashed-dotted line corresponds to the best fit to the experimental isomer ratio obtained by using the all-angular-momenta approximation with $\sigma = 5$, whereas the short-dashed line represents the results obtained with the high-angular-momenta approach with $\sigma = 3$.

c.m. energies have to be well below the Coulomb barrier. In this case, it would be quite unlikely to populate the $25/2^+$ isomeric state in ^{211}Po. However, the discrepancies between the theoretical results calculated with the all-angular-momenta approximation and measured isomer ratio is, in the worst case, less than a factor of 2 in the region where the $2n$ evaporation channel is predominant [see for example Fig. 5(a)]. By adopting the all-angular-momenta approximation with angular momentum spread $\sigma = 5$, it is possible to describe the ^{211}Po isomer ratio obtained from the $t+^{209}$Bi ICF

reaction to a level similar to that in the ^{212}At case, as illustrated by the dashed-dotted line in Fig. 12(b). The results of the high-angular-momenta calculations (short-dashed line), obtained with $\sigma = 3$, are also compared with the measured isomer ratio in the same figure. As expected, the overall agreement between data and calculation is somewhat less satisfactory in comparison with the results provided by the all-angular-momenta approximation. This behavior is consistent with all the other isomer ratio results presented in this paper.

[1] M. Dasgupta, D. J. Hinde, N. Rowley, and A. M. Stefanini, Annu. Rev. Nucl. Part. Sci. **48**, 401 (1998).

[2] I. J. Thompson and A. Diaz-Torres, Prog. Theor. Phys. Suppl. **154**, 69 (2004).

[3] A. Mukherjee, U. Datta Pramanik, M. Saha Sarkar, A. Goswami, P. Basu, S. Bhattacharya, S. Sen, M. L. Chatterjee, and B. Dasmahapatra, Nucl. Phys. **A596**, 299 (1996).

[4] A. Mukherjee, U. Datta Pramanik, S. Chattopadhyay, M. Saha Sarkar, A. Goswami, P. Basu, S. Bhattacharya, M. L. Chatterjee, and B. Dasmahapatra, Nucl. Phys. **A635**, 305 (1998).

[5] A. Mukherjee, U. Datta Pramanik, S. Chattopadhyay, M. Saha Sarkar, A. Goswami, P. Basu, S. Bhattacharya, M. L. Chatterjee, and B. Dasmahapatra, Nucl. Phys. **A645**, 13 (1999).

[6] V. Tripathi, A. Navin, K. Mahata, K. Ramachandran, A. Chatterjee, and S. Kailas, Phys. Rev. Lett. **88**, 172701 (2002).

[7] V. Tripathi, A. Navin, V. Nanal, R. G. Pillay, K. Mahata, K. Ramachandran, A. Shrivastava, A. Chatterjee, and S. Kailas, Phys. Rev. C **72**, 017601 (2005).

[8] D. E. DiGregorio, J. O. Fernández Niello, A. J. Pacheco, D. Abriola, S. Gil, A. O. Macchiavelli, J. E. Testoni, P. R. Pascholati, V. R. Vanin, R. Liguori Neto, N. Carlin Filho, M. M. Coimbra, P. R. Silveira Gomes, and R. G. Stokstad, Phys. Lett. **B176**, 322 (1986).

[9] D. E. DiGregorio, M. diTada, D. Abriola, M. Elgue, A. Etchegoyen, M. C. Etchegoyen, J. O. Fernández Niello, A. M. J. Ferrero, S. Gil, A. O. Macchiavelli, A. J. Pacheco, J. E. Testoni, P. R. Silveira Gomes, V. R. Vanin, R. Liguori Neto, E. Crema, and R. G. Stokstad, Phys. Rev. C **39**, 516 (1989).

[10] S. Gil, D. Abriola, D. E. DiGregorio, M. di Tada, M. Elgue, A. Etchegoyen, M. C. Etchegoyen, J. Fernández Niello, A. M. J. Ferrero, A. O. Macchiavelli, A. J. Pacheco, J. E. Testoni, P. Silveira Gomes, V. R. Vanin, A. Charlop, A. Garcia, S. Kailas, S. J. Luke, E. Renshaw, and R. Vandenbosch, Phys. Rev. Lett. **65**, 3100 (1990).

[11] P. R. S. Gomes, I. C. Charret, R. Wanis, G. M. Sigaud, V. R. Vanin, R. Liguori Neto, D. Abriola, O. A. Capurro, D. E. DiGregorio, M. di Tada, G. Duchene, M. Elgue,

A. Etchegoyen, J. O. Fernández Niello, A. M. J. Ferrero, S. Gil, A. O. Macchiavelli, A. J. Pacheco, and J. E. Testoni, Phys. Rev. C **49**, 245 (1994).

[12] M. di Tada, D. E. DiGregorio, D. Abriola, O. A. Capurro, G. Duchêne, M. Elgue, A. Etchegoyen, J. O. Fernández Niello, A. M. J. Ferrero, A. J. Pacheco, P. R. Silveira Gomes, and J. E. Testoni, Phys. Rev. C **47**, 2970 (1993).

[13] C. Signorini, Z. H. Liu, A. Yoshida, T. Fukuda, Z. C. Li, K. E. G. Löbner, L. Müller, Y. H. Pu, K. Rudolph, F. Soramel, C. Zotti, and J. L. Sida, Eur. Phys. J. A **2**, 227 (1998).

[14] M. Dasgupta, D. J. Hinde, R. D. Butt, R. M. Anjos, A. C. Berriman, N. Carlin, P. R. S. Gomes, C. R. Morton, J. O. Newton, A. Szanto de Toledo, and K. Hagino, Phys. Rev. Lett. **82**, 1395 (1999).

[15] M. Dasgupta, D. J. Hinde, K. Hagino, S. B. Moraes, P. R. S. Gomes, R. M. Anjos, R. D. Butt, A. C. Berriman, N. Carlin, C. R. Morton, J. O. Newton, and A. Szanto de Toledo, Phys. Rev. C **66**, 041602(R) (2002).

[16] M. Dasgupta, P. R. S. Gomes, D. J. Hinde, S. B. Moraes, R. M. Anjos, A. C. Berriman, R. D. Butt, N. Carlin, J. Lubian, C. R. Morton, J. O. Newton, and A. Szanto de Toledo, Phys. Rev. C **70**, 024606 (2004).

[17] R. Vandenbosch, Annu. Rev. Nucl. Part. Sci. **42**, 447 (1992).

[18] A. R. Barnett and J. S. Lilley, Phys. Rev. C **9**, 2010 (1974).

[19] W. J. Ramler, J. Wing, D. J. Henderson, and J. R. Huizenga, Phys. Rev. **114**, 154 (1959).

[20] A. B. Balantekin and P. E. Reimer, Phys. Rev. C **33**, 379 (1986).

[21] K. Hagino, N. Rowley, and A. T. Kruppa, Comput. Phys. Commun. **123**, 143 (1999).

[22] H. Ikezoe, N. Shikazono, Y. Tomita, K. Ideno, Y. Sugiyama, and E. Takekoshi, Nucl. Phys. **A444**, 349 (1985).

[23] A. Diaz-Torres, D. J. Hinde, J. A. Tostevin, M. Dasgupta, and L. R. Gasques, (submitted to Phys. Rev. Lett).

[24] D. J. Hinde, M. Dasgupta, B. R. Fulton, C. R. Morton, R. J. Wooliscroft, A. C. Berriman, and K. Hagino, Phys. Rev. Lett. **89**, 272701 (2002).